SAN ROSSORE (ITALY) FORESTRY TEST SITE: METHODOLOGY FOR CALIBRATION AND VALIDATION OF CHRIS-PROBA DATA

Alessandro Barducci[(1)], Francesco Castagnoli[(1)], Donatella Guzzi[(1)], Paolo Marcoionni[(1)], Ivan Pippi[(1)]

[(1)]National Research Council –Applied Physics Institute "Nello Carrara"
via Panciatichi 64, 50127 FIRENZE, ITALY - I.Pippi@ifac.cnr.it

ABSTRACT

Following the general trend to better understand the directional reflection properties of a surface, we present some results from CHRIS-PROBA images acquired during last year over the San Rossore (Italy) forestry test site. Particular attention is devoted to the description of the adopted methodology for calibrating and validating CHRIS-PROBA data and for obtaining images of spectral reflectance taking into account the atmospheric effects. Anisotropy Factor are estimated from experimental data and they are used in conjunction of literature data to study the spectral behaviour of multiangle remotely sensed data.

1. INTRODUCTION

A large amount of laboratory and in-field measurements has been collected in order to assess the geometrical properties of reflection from a surface in terms of Bi-Directional Reflectance Distribution Function (BRDF).
This quantity, which takes into account both the illumination and the viewing geometry [1], describes the directional reflectance by relating the incident irradiance from a given pencil of directions to its contribution to the reflected radiance in another propagation direction. To this aim various systems have been developed such as the European GOniometric Facility (EGO) by the Joint Research Centre (Ispra, Italy) [2], the LAbor-GOniometer System (LAGOS) and FIeld-GOniometer System (FIGOS) by the University of Zurich [3], the Portable Apparatus for Rapid Acquisition of Bidirectional Observation of Land and Atmosphere (PARABOLA) instrument by NASA – GSFC [4], and an instrument manufactured at Miami University (Florida, USA), which is able to perform simultaneously multiple viewing-angle measurements [5].
Moreover, recent satellite missions such as the Multi-angle Imaging SpectroRadiometer (MISR) on the Earth Observation Science (EOS AM-1) Terra platform [6] and the Compact High Resolution Imaging Spectrometer (CHRIS) on board of European Space Agency (ESA) PRoject for On Board Autonomy 1 (PROBA-1) platform [7] supply experimenters with their off-nadir viewing capability.
Following this general trend aimed to improve the current understanding of directional properties of reflection from natural surfaces, we present a large CHRIS-PROBA data set acquired over the San Rossore (Italy) forestry test site during the last year.
This sample area is included within the Regional Natural Park of Migliarino-San Rossore- Massacciucoli and it is characterised by a land cover mainly dominated by the presence of *Pinus pinaster* Ait., and *Pinus pinea* L.. This Park is close to the shoreline and it includes the Arno and Serchio river's estuary.
Inside the San Rossore area many groups are involved in different research activities dealing with agronomy, climatology, eco-physiology and they often utilise remote sensing techniques. For this aim many efforts are devoted to the calibration and validation of aerospace hyperspectral data. In order to obtain level 2 products by correcting remote sensing data for atmospheric effects San Rossore area has been permanently equipped with scientific instruments which measure total and diffuse solar irradiance in the visible and infrared spectral range, ground temperature, pressure, relative humidity.
After introducing some details about CHRIS spectrometer in Section 2, the description of the calibration and validation procedure is reported in Section 3 together with a preliminary data quality assessment of CHRIS-PROBA data. Section 4 is devoted to the presentation of early results obtained correcting the experimental data for the atmospheric effects. In Section 5 conclusion and open problem are drawn with the discussion of future activities to be carried out in order to better assess BRDF effects from multiangle remotely sensed data.

2. CHRIS SPECTROMETER

CHRIS is a "push-broom" imaging spectrometer that was designed by SIRA Electro-Optics Ltd. (U.K.) to collect data for land investigation and aerosol measurement. CHRIS is the main instrument payload on ESA small satellite platform PROBA-1 launched on October 22, 2001.
The mission is being used as a demonstrator in order to evaluate the performance of compact design technology. The knowledge derived from CHRIS-PROBA will guide the design of hyperspectral imaging systems for future missions, such as the ESA Earth Explorer Mission SPECTRA.
The main scientific CHRIS-PROBA goal is the measurement of Earth surface directional reflectance in the visible and near-infrared spectral bands using the platform pointing capability.

Proc. of the 2nd CHRIS/Proba Workshop, ESA/ESRIN, Frascati, Italy
28-30 April (ESA SP-578, July 2004)

To this aim in the along-track and across-track directions CHRIS acquires a set of five images of the same scene during the same sun-synchronous polar orbit. Each image set has an associated "fly-by position" on the ground (roughly the image center) that corresponds to the Minimum Zenith Angle (MZA), defined as the off-nadir inclination of the sensor viewing direction in the plane perpendicular to the satellite orbit. The line of sight inclination in the along track direction (held in the orbit plane) is indicated by the Fly-by Zenith Angle (FZA). The geometrical composition of the aforementioned angles gives the true zenith angle of the sensor viewing direction.

CHRIS acquires images of the same scene at FZA of $+55^o$, $+36^o$, 0^o, -36^o, and -55^o during the same orbit with different configurations. In fact, CHRIS collects 18, 37 or 63 spectral bands if operated at spatial resolution of 18 or 36 m with a spectral coverage ranging from 405 nm until 1050 nm. The main characteristics of CHRIS spectrometer are listed in Table I.

Table 1. Main characteristics of CHRIS-PROBA.

Instrument:	push-broom imaging spectrometer
Field of view:	1.3^o
Ground swath:	13.5 km
Altitude:	Apogee: 688 km, perigee: 556 km
Orbit inclination:	97.8^o
Descending node:	12:10 local time
Across track pixel size:	18m or 36m
Along track pixel size:	Finest resolution is 18m
Number of images:	5 acquisitions of the same area at +55, +36, 0, -36, -55 view angles during the same orbit
Spectral range:	410 nm to 1050 nm
Spectral resolution:	From 1.25 nm @ 400 nm to 11 nm @ 1050 nm and binning possibility
Number of spectral bands	From 18 bands at a spatial resolution of 18 m, to 63 at 36m
Digitalization	12 bits
Signal-to-noise ratio	max. 250 @ target albedo = 0.2, λ = 800 nm, gain = 8.583

Since June 2002 up to now many hyperspectral images were collected over San Rossore forestry test site (latitude: 43.73^o N, longitude: 10.30^o E, altitude 5 meters a.s.l.) by CHRIS utilizing different spectral configuration (MODE) and for various angular geometries.

Table II lists the complete set of images acquired so far.

Table 2. Complete list of CHRIS images acquired so far over the San Rossore forestry test site.

	DATE and TIME (GMT)	MZA	MODE
1	June 19, 2002 10:27	-6^o	4
2	April 16, 2003 10:41	-19^o	4
3	June 16, 2003 10:32	0^o	4
4	July 1, 2003 10:26	$+13^o$	4
5	July 25, 2003 10:34	-2^o	3
6	August 25, 2003 10:32	$+4^o$	30
7	September 18, 2003 10:37	-8^o	3
8	October 12, 2003 10:42	-16^o	3
9	October 19, 2003 10:31	$+5^o$	3
10	January 15, 2004 10:34	-6^o	3
11	February 9, 2004 10:43	-15^o	3
12	March 27, 2004 10:26	$+18^o$	3

3. CALIBRATION AND VALIDATION METHODOLOGY OF CHRIS-PROBA DATA

3.1 Physical background

The geometrical properties of a reflecting surface are readily described by its BRDF, denoted symbolically as $\rho_{BRDF}(\lambda,\vartheta_0,\phi_0,\vartheta_r,\phi_r)$, which is defined [1] as the ratio of the radiance $dL^{out}(\lambda,\vartheta_0,\phi_0,\vartheta_r,\phi_r;E_i)$ scattered into the direction (ϑ_r,ϕ_r) to the irradiance $dE_i(\lambda,\vartheta_0,\phi_0)$ impinging at angle (ϑ_0,ϕ_0) on a unitary surface area:

$$\rho_{BRDF}(\lambda,\vartheta_0,\phi_0,\vartheta_r,\phi_r)=\frac{dL^{out}(\lambda,\vartheta_0,\phi_0,\vartheta_r,\phi_r;E_i)}{dE_i(\lambda,\vartheta_0,\phi_0)} \quad (1)$$

As indicated in Eq. 1 BRDF is a density of reflectance [sr^{-1}] ranging from zero to infinity. Let us note that the BRDF, defined as ratio of infinitesimals (vanishing quantities), is a derivative with instantaneous values that can not be directly measured, since real measurements involve finite extension intervals (resolution) of the concerned geometrical parameters.

Although the BRDF is an important parameter for describing the surface reflectance, its measurement is hindered even for simple surfaces from the impossibility of yielding Field-Of-View (FOV) having a vanishing width. Moreover, because this function varies versus both illumination and viewing angle, many measurements are required for laboratory reflectance measurements.

A common simplification of the BRDF is to assume the concerned reflector as a Lambertian (perfectly diffuser) surface, i.e. an infinite ideal surface for which the reflected radiance is isotropic with the same value for all directions (ϑ_v,ϕ_v) regardless of how it is irradiated. Therefore, Lambertian surfaces constitute a restricted ensemble of reflectors, which are included in the more general class of natural surfaces. For Earth remote sensing purpose, spectral reflectance is generally retrieved considering the observed target as a Lambertian and homogeneous diffuser for which the upward radiance can explicitly be expressed as a function of surface reflectance [8], [9].

In the visible and near-infrared spectral range, the reflectance of an observed Lambertian surface is retrieved using the well-known Eq. 2:

$$\rho(\lambda) = \frac{\pi[L_{1B}(\lambda,\vartheta) - L_{path}(\lambda,\vartheta)]}{T(\lambda,\vartheta)E_{tot}(\lambda,\zeta)} \frac{1}{\cos\vartheta} \quad (2)$$

where ϑ is the zenith angle of the viewing direction, ζ the Sun's zenith distance, $L_{1B}(\lambda,\vartheta)$ the spectral radiance reaching the sensor, $E_{tot}(\lambda,\zeta)$ the total (direct plus diffuse) irradiance impinging on the target, $L_{path}(\lambda,\vartheta)$ the atmospheric up-welling "path radiance", and $T(\lambda,\vartheta)$ the atmospheric transmittance from ground to the sensor. Each spectral term in the right side of Eq. 2 is intended to be averaged over the spectral channel bandwidth, while the geometrical factor $\cos\vartheta$ only accounts for the push-broom imaging spectrometer sampling.

Although many surfaces behave similarity to an ideal diffuser, the above assumption will fail in two areas. The first obvious failure is that many flat surfaces have a not negligible specular component (for instance oceanic water in the visible spectral range and high-reflecting soil), i.e. an increase in the observed reflectance when the illumination and viewing zenith angles are the same and the relative azimuth angle is 180°.

Many rough surfaces (like vegetation) also show a reflectance increase in the "hot spot" direction when the illumination and viewing zenith angles are the same but the relative azimuth angle is null. Moreover, the error resulting from assuming Lambertian reflection for a natural target can be large for off-nadir views in remote sensing observations [10], [11].

However, it is possible to define another class of reflectors whose bi-directional reflectance distribution function $\rho_{BRDF}(\lambda,\vartheta_i,\phi_i,\vartheta_v,\phi_v)$ is assumed to be a separable function in spectral and geometrical factors as shown in Eq. 3:

$$\rho_{BRDF}(\lambda,\vartheta_i,\phi_i,\vartheta_v,\phi_v) \approx \rho_0(\lambda)h(\vartheta_i,\phi_i,\vartheta_v,\phi_v) \quad (3)$$

If we impose according to the definition of reflected irradiance [1] that:

$$\int_{2\pi_v} h(\vartheta_i,\phi_i,\vartheta_v,\phi_v)\cos\vartheta_v d\Omega_v = \pi \quad (4)$$

then, we obtain an additional definition of albedo $\rho_0(\lambda)$:

$$\rho_0(\lambda) = \frac{\int_{2\pi_v} \rho_{BRDF}(\lambda,\vartheta_i,\phi_i,\vartheta_v,\phi_v)\cos\vartheta_v d\Omega_v}{\pi} \quad (5)$$

being $\cos\vartheta_v d\Omega_v$ the so called projected solid angle.

3.2 Data quality assessment

Every "push-broom" imaging spectrometer is affected by along-track stripes changing with wavelength, and the response corrected images, as provided by SIRA, have to be corrected for this kind of disturbance. In absence of any flat-field calibration measurement, an empirical correction algorithm has been adopted to remove this effect [12]. This algorithm is able to separate contributions due to scene texture from those originated by the noise pattern utilizing information from the acquired image data alone (average image horizontal line).

A statistical data quality assessment of at-sensor radiance spectra has also been performed analyzing image minimum, maximum and mean values as well as its standard deviation, skewness, energy and entropy. Particular attention has been devoted to the calculation of radiometric levels (histograms) for each image in order to establish the effective dynamic range of the sensor.

4. PRELIMINARY RESULTS

4.1 Noise removal and statistical computation

In Fig.1 at-sensor radiance image acquired by CHRIS over San Rossore on September 18, 2003 is shown. The viewing geometry is specified by MZA = -8° and FZA = 0° with a solar zenith angle (SZA) of 43°.

As can be seen, this image is affected by the so called "stripe-noise" which appears as vertical lines superimposed to the observed scene.

Fig. 2 shows the same image corrected for this coherent noise applying. The average image brightness has not been changed but the noise pattern has been strongly reduced.

Fig. 1. at-sensor radiance image acquired by CHRIS over San Rossore on September 18, 2003 with MZA = -8° and FZA = 0°. The image is displayed in "true colors": Red channel (6th band, 631 nm), Green channel (3rd band, 530 nm) and Blue channel (1st band, 442 nm).

Fig. 2. Same image of Fig.1 after correcting the "stripe-noise". The vertical lines are strongly reduced.

Simulations of at-sensor radiance have been performed utilizing MODTRAN 4 in order to compare the obtained spectra with those extracted from various CHRIS image. Fig. 3 shows the comparison among these spectra from beach sand surface (located south, near the Gombo residence) whose reflectance spectrum was measured in laboratory and used to run MODTRAN 4.
As can be seen the agreement between simulations and measurements appears to be fair even if the experimental data are systematically lower than those simulated, and some degradation of the sensor response is detected especially at both ends of the observed spectral range.

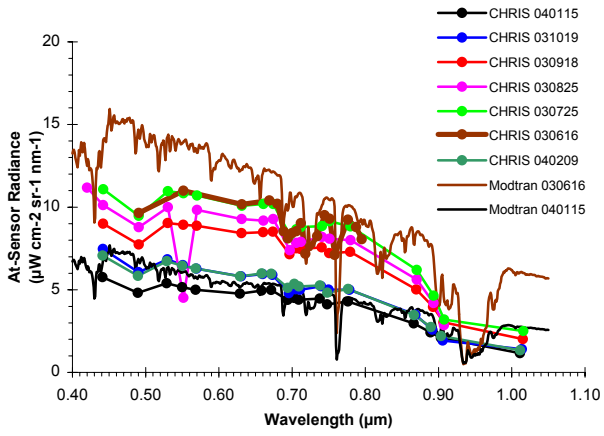

Fig. 3. Comparison between MODTRAN 4 radiance spectra from beach sand surface and CHRIS spectra extracted from the same pixel.

This circumstance is also confirmed by the analysis of statistical values computed from response corrected images as provided by SIRA. In Table 3 statistical values related to the CHRIS image gathered at FZA = 0° on June 16, 2003 are reported.

Table 2. Statistical values related to the CHRIS image acquired at FZA = 0° on June 16, 2003 over San Rossore forestry test site.

Band	Nlev	Min	Max	Mean	St.Dev.
1	33914	47625	157623	64745.58	6820.558
2	45644	39583	179964	58979.36	11526.70
3	58192	23050	176374	40849.03	15269.64
4	60928	19971	178412	37641.57	16589.53
5	61416	18818	175738	36184.67	16561.83
6	56327	15188	150080	31252.90	14543.23
7	55844	15063	142770	30818.22	14365.86
8	57841	14749	143724	32671.80	15549.19
9	59844	14994	151241	36168.03	17792.08
10	60624	14515	154872	39015.17	19950.56
11	51903	-3839	393653	35602.87	19186.81
12	63882	-15241	162835	47098.83	29008.73
13	78260	-3279	347597	57008.36	37962.56
14	81974	-4265	381573	57837.91	39565.20
15	68858	-4112	141037	45126.86	31089.23
16	84749	-12606	317160	58304.07	41541.18
17	82771	-3933	299149	55747.09	40088.34
18	78379	-3705	397534	51731.65	37375.24

As can be seen, some spectral channels have negative minima and a too high number of radiometric levels with respect to the sensor dynamic range (12 bit).

4.2 Atmospheric effects correction

Fig. 3 shows an example of reflectance map retrieved from CHRIS images after the atmospheric correction depicted in Eq. 2 including restoration from trapping effect. The image was acquired by CHRIS over San Rossore on July 25, 2003 at 10 34 GTM, with a spatial resolution of 18 m and gathered at MZA = -2° and FZA = +36°. The Solar Zenith Angle (SZA) was 26° and the Solar Azimuth Angle (SAA) was 152°

Fig. 3. Reflectance image displayed in "true color", like in Fig.1, as result of data acquired July 25, 2003 at MZA = -2° and FZA = +36°.

In Fig.s 4(a)-(c) we show spectra of reflectance obtained at different viewing geometries for the same ground location. Sand, vegetation and sea surface data have been extracted from the five images set of 25 July and plotted in separate pictures.

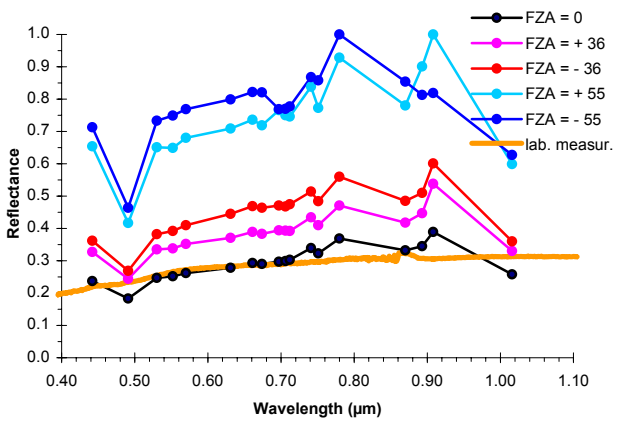

(a)

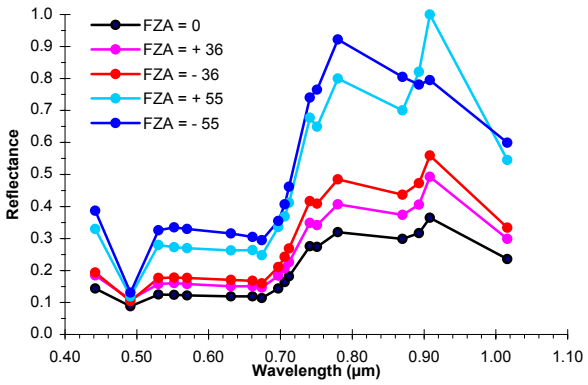

(b)

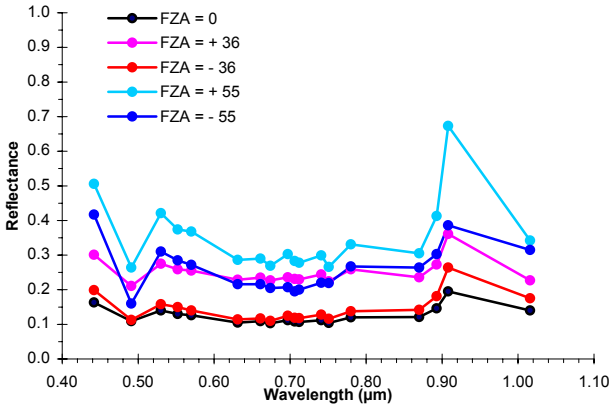

(c)

Fig. 4. Examples of reflectance spectra obtained from CHRIS images acquired on July 25, 2003. Each spectra set was extracted from the same ground location (a) sand, (b) vegetation and (c) sea pixel (about two km far from the coast line). Nadir sand spectra (FZA=0°) can be compared to the spectra of the same sand sample measured in laboratory.

In Fig.4(a) sand reflectance is compared with reflectance measurement carried out in laboratory over the same sample. Let us note the good agreement between the laboratory measurement and the nadir spectrum with a residual relative difference which is lower than 15 % at the both ends of the digitised spectral range. The spectral region of worst agreement (around 0.760 µm) is characterised for inherent difficulty in atmospheric modelling that may involve inaccuracy in the adopted O_2 absorption band model. Another trouble that may affect spectral matching between the two reflectance estimates is due to poor radiometric calibration of CHRIS sensor especially at both ends of the observed spectral range.

In order to elucidate spectral behaviour of multiangle remotely sensed data in Fig.s 5(a)-(c) we have reported reflectance normalized to that obtained at nadir viewing geometry (with FZA = 0°).

The anisotropy factor (ANIF) resulting from this normalization technique, which is applicable when a low angular resolution of directional data is available like in CHRIS data set, is a tool to separate directional effects from spectral signature of the involved surface according to the following definition:

$$\rho_{ANIF}(\lambda,\vartheta_0,\phi_0,\vartheta_r,\phi_r) = \frac{\rho\ (\lambda,\vartheta_0,\phi_0,\vartheta_r,\phi_r)}{\rho\ (\lambda,\vartheta_0,\phi_0,0)} \qquad (6)$$

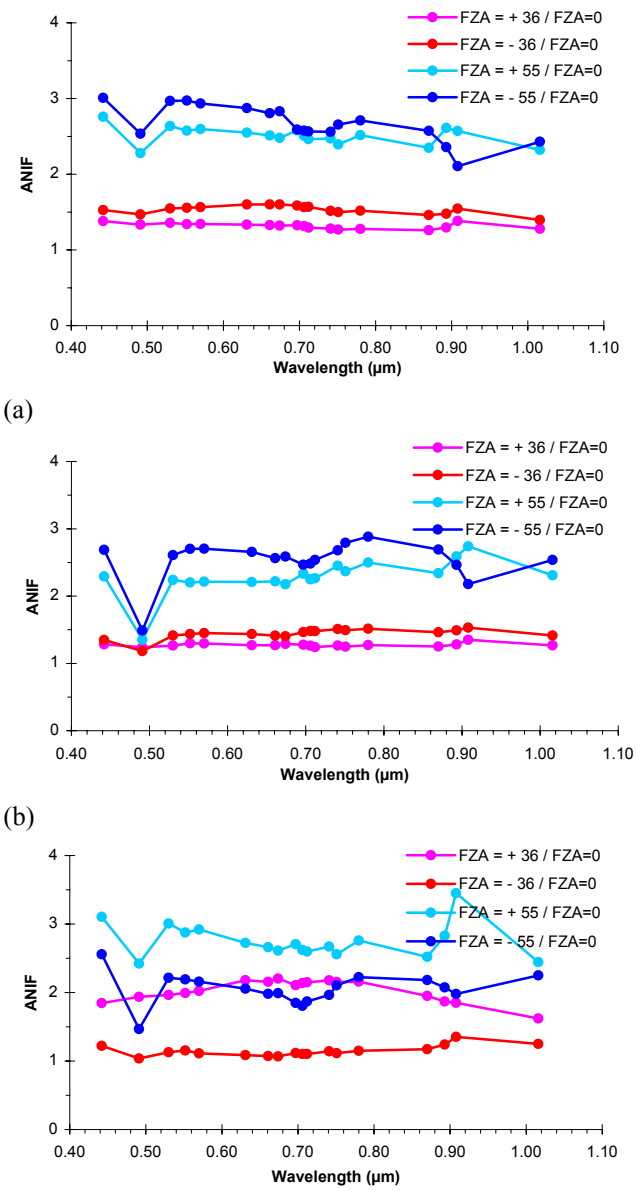

Fig. 5. Examples of reflectance normalized to that obtained at nadir viewing geometry (with FZA = 0°) for data shown in Fig. 4.for (a) sand, (b) vegetation and (c) sea pixel (about two km far from the coast line).

Anisotropy factors are plotted versus viewing zenith angles in Fig.s 6(a)-(c) for six different wavelengths related to the July acquisition for the same natural targets (sand, vegetation and sea).

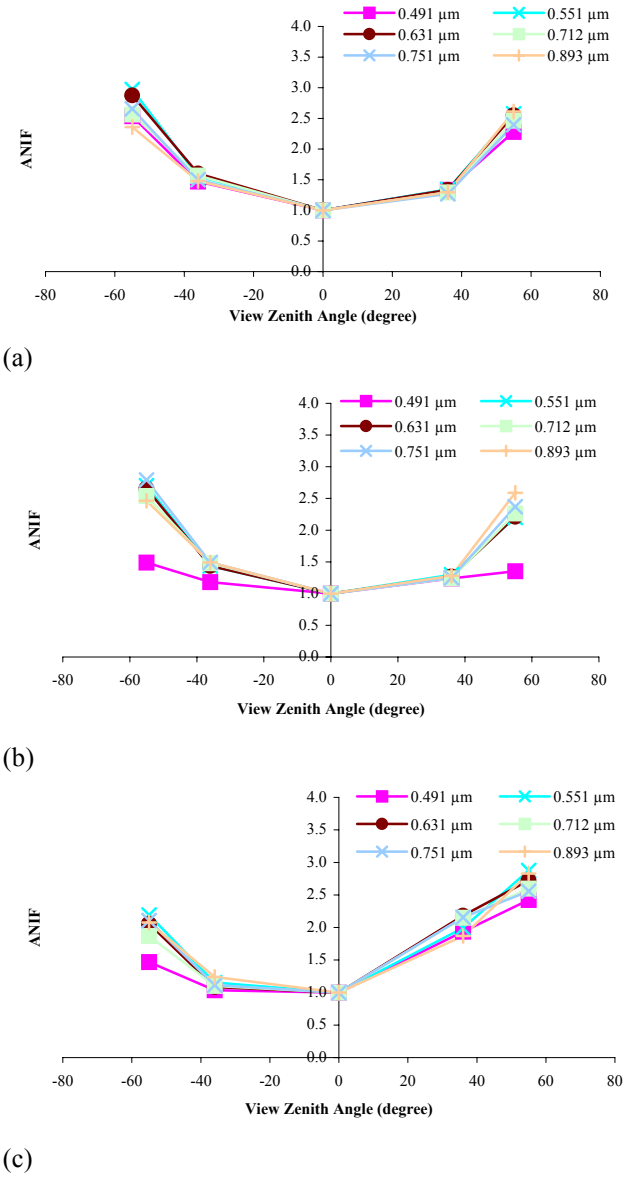

Fig. 6. Anisotropy factors versus viewing zenith angles are shown for six different wavelengths (0.491 µm, 0.552 µm, 0.631 µm, 0.712 µm, and 0.893 µm) related to the July acquisition for the same ground location (a) sand pixel,(b) vegetation pixel and (c) sea pixel (about two km far from the coast line). The forward (backward) direction is indicated by positive (negative) values for viewing zenith angles.

As can be seen the estimated reflectance factors show a distinct spectral behaviour for different targets. Over sand all six wavelengths show a fairly symmetrical bowl shape. Over vegetation the bowl shape is particularly well developed in the near-infrared wavelengths while in the blue and red chlorophyll absorption band directional effects are more pronounced.

The observed spectral dependence of directional reflectance may be explained considering the relationship

between vegetation canopy optical properties and multiple scattering effects [13], [14].
In the high absorbing (low reflecting) wavelengths located at 0.491 μm and 0.631 μm, multiple scattering effects are reduced due to a low amount of radiation travelling inside the vegetation canopy. Therefore, the contrast between shadowed and illuminated canopy components, and consequently the BRDF effects are enhanced.
In the green wavelength at 0.551 μm and, particularly, in the near-infrared wavelengths at 0.751 μm and 0.893 μm, multiple scattering effects are strong since the corresponding average single-scattering albedo is relatively high and, therefore, directional effects are dimmed. As a consequence, BRDF effects are rather small in the low-absorbing (high reflecting) wavelengths.
In Fig. 6(a) the estimated reflectance factors show a fairly symmetrical bowl shape since the corresponding spectral single-scattering albedo increases with wavelength but the change is small.
As shown in Fig. 6(b) in the backward direction (negative values of FZA) it is evident the "hot spot" phenomenon, which is caused by the absence of shadow in the radiation scattered back toward the source. As observed this effect is more pronounced at blue (0.491 μm) and red wavelengths (0.631 μm). In the near-infrared wavelengths (0.751 μm and 0.893 μm) the larger amount of multiple scattering reduces "hot spot" but increases reflectance at high view zenith angles.
Over sea surface, see Fig. 6(c), the anisotropy factor is dominated by specular reflection in the forward directions (positive values of FZA) as it also evident from Fig. 3.
Fig.7 shows the behaviour of vegetation anisotropy factor computed at 0.491 μm wavelength for three different values of SZA.

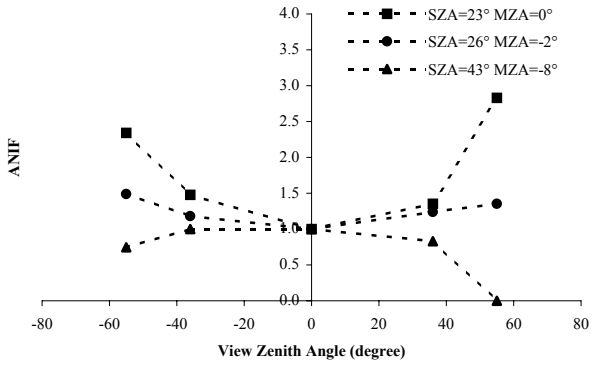

Fig. 7. Anisotropy factors versus viewing zenith angles for three different values of solar zenith angles (SZA). The factor is computed at 0.491 μm of wavelength for vegetation canopy.

As can be seen, the "hot spot" peak is more pronounced for small solar zenith angles (at SZA=23^o, and SZA=26^o). The reason for this behaviour may be connected to the circumstance that for small solar zenith angles the optical path is relatively small and the probability to collect radiance back-scattered toward the source without encountering any other scatterer is large. Conversely, for high zenith solar angles most of contribution to at-sensor radiance comes from multiple scattering that in turns reduce the hot-spot effect.
Monochromatic ANIF images have been computed starting from the CHRIS data set of July 25, and an example of this processing has been shown in Fig.8 for the 2nd CHRIS spectral channel (0.491 μm). The image has been obtained as the ratio between two target reflectances estimated from images at FZA=+36^o and FZA=0^o. To this aim the off-nadir (FZA=+36^o) image was precisely geo-located with respect to the nadir (FZA=0^o) acquisition, using the ENVI second-degree polynomial co-registration procedure based on 40 ground control points (GCP). The r.m.s. error for the considered GCPs as estimated from the procedure was about 0.8 pixel, a circumstance that confirms the high accuracy of the performed geo-location.

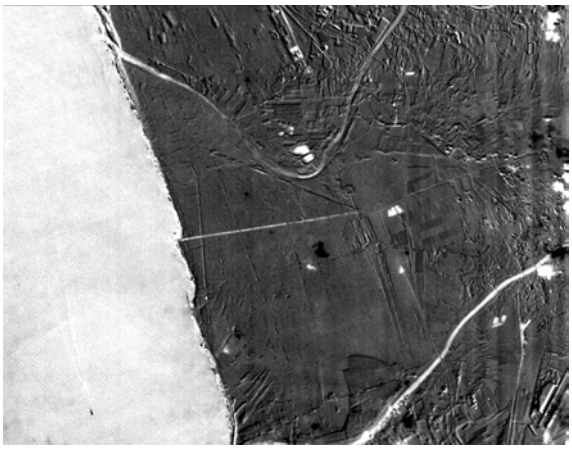

Fig. 8. Monochromatic ANIF images computed from CHRIS data set acquired on July 25, and displayed utilising the 2nd CHRIS spectral channel (0.491 μm).

We point out that the outcome of ANIF calculation is a flat image in which the difference among different targets is subtle. The picture in Fig. 8, in fact, reminds typical thermal infrared images where one can only observe small signal variations along the scene. It can be seen that homogeneous areas of the original data of Fig. 3 give rise to grey regions in Fig.8, and that different kinds of vegetation coverage are no longer detectable in the ANIF domain. We have verified that the ANIF maps computed at different wavelengths originate roughly the same image shown in Fig. 8, confirming that the ANIF signal has high spectral correlation.

5. CONCLUSIONS

In this paper some results, obtained from multiangle images acquired by CHRIS over the San Rossore (Italy) site during the last year, have been presented. A deep investigation about reflectance dependence on optical

properties of the surface, illumination and viewing geometry has been performed by estimating anisotropy factor from the available multiangle data sets. From the analysis of this great amount of data the spectral variability of the retrieved factors has been assessed versus viewing zenith angles. Physical mechanism have been proposed in conjunction with already existing scientific works to explain the observed spectral behaviour of remotely sensed data.
The need to improve the modelling of BRDF of natural surface has arisen from the analysis of preliminary results and future investigations will regard the effects of atmosphere on the retrieval of reflectance from multiangle remote sensing data.

6. AKNOWLEDGMENTS

We would like to thank all the scientists from different institutions that are involved in remote sensing activities carried out in San Rossore test site. Moreover, we would like to thank people from SIRA and RSAC in particular M. Cutter and P. Fletcher for planning the acquisitions and providing CHRIS data, and for useful discussions.

7. REFERENCES

1. Nicodemus, F., E., Richmond, J., C., Hsia, J., J., Ginsberg, I., W., and Limperis, T., Geometrical considerations and nomenclature for reflectance, *Technical Report NBS MN-160*, National Bureau of Standards, 1977.

2. Sandmeier, S., Muller, C., Hosgood, B., Andreoli, G., Sensitivity Analysis and Quality Assessment of Laboratory BRDF data, *Remote Sensing of Environment*, Vol. 64, pp. 176 – 191, 1998.

3. Sandmeier, S., Itten, I., K., A field goniometer system (FIGOS) for acquisition of hyperspectral BRDF data, *IEEE Transactions on Geoscience and Remote Sensing*, Vol. 37, No. 2, pp. 978 – 986, 1999.

4. Deering, D., W., and Leone, P., A sphere-scanning radiometer for rapid directional measurements of sky and ground radiance, *Remote Sensing of Environment*, Vol. 19, pp. 1 – 24, 1986.

5. Voss, K., J., Chapin, A., Monti, M., and Zhang, H., Instrument to measure the bi-directional reflectance distribution function of surfaces, *Applied Optics*, Vol. 39, No. 33, pp. 6197 – 6206, 2000.

6. Diner, D., J., Beckert, J., C., Reilly, T., H., Bruegge, C., J., Conel, J., E., Kahn, R., A., Martonchik, J., V., Ackerman, T., P., Davies, R., W. Gerstl, S., A., Gordon, H., R., Muller, J-P., Myneni, R., B., Sellers, P., J., Pinty, B., and Verstraete, M., M., Multi-angle Imaging SpectroRadiometer (MISR) instrument description and experiment overview, *IEEE Transactions on Geoscience and Remote Sensing*, Vol. 36, pp. 1072 – 1087, 1998.

7. Cutter, M., A., Johns, L., S., Lobb, D., R., Williams, T., L., Settle, J., J., Flight Experience of the Compact High Resolution Imaging Spectrometer (CHRIS), *Proceeding of SPIE Conference 5159 Imaging Spectrometry IX, August 2003, San Diego, California, USA*, 2003

8. Barducci, A., Pippi, I., Atmospheric Effects Evaluation for the AVIRIS Image-Data Correction or Retrieval, *Proceeding of SPIE – Recent Advances in Remote Sensing and Hyperspectral Remote Sensing, EUROPTO Series*, 2318, pp. 10 – 16, 1994.

9. Qiu, J., An improved model of surface BRDF-atmospheric coupled radiation, *IEEE Transactions on Geoscience and Remote Sensing*, Vol. 39, n. 1, pp. 181 – 187, 2001.

10. Martonchik, J., V., Davide, J., D., Pinty, B., Verstraete, M., M., Myneni, R., B., Knyazikhin, Y., and Gordon, R., Determination of Land and Ocean Reflective, Radiative, and Biophysical Properties Using Multiangle Imaging, *IEEE Transactions on Geoscience and Remote Sensing*, Vol. 36, No. 4, pp. 1266 – 1281, 1998.

11. Miesch, C., X., Briottet, and Kerr, Y., Bidirectional reflectance of a rough anisotropic surface, *Internation Journal of Remote Sensing*, Vol. 23, No. 15, pp. 3107 – 3114, 2002.

12. Barducci, A., and Pippi, I. Analysis and rejection of systematic disturbances in hyperspectral remotely sensed images of the Earth. *Applied Optics*, 40, 1464 – 1477, 2001.

13. Pinty, B., Ramond, D., A simple bi-directional reflectance model for terrestrial surfaces, *Journal of Geophysical Research*, Vol. 91, No. D7, pp. 7803 – 7808, 1986.

14. Ahmad, S. P., and Deering, D. W., A simple analytical function for bi-directional reflectance. *Journal of Geophysical Research*, 97, 18867 – 18886, 1992.